NANO LETTERS

pubs.acs.org/NanoLett Letter

# Controlling Nanoparticle Uptake in Innate Immune Cells with Heparosan Polysaccharides

Wen Yang, Alex N. Frickenstein, Vinit Sheth, Alyssa Holden, Evan M. Mettenbrink, Lin Wang, Alexis A. Woodward, Bryan S. Joo, Sarah K. Butterfield, Nathan D. Donahue, Dixy E. Green, Abigail G. Thomas, Tekena Harcourt, Hamilton Young, Mulan Tang, Zain A. Malik, Roger G. Harrison, Priyabrata Mukherjee, Paul L. DeAngelis, and Stefan Wilhelm*

Cite This: https://doi.org/10.1021/acs.nanolett.2c02226 Read Online

ACCESS | Metrics & More | Article Recommendations | Supporting Information

**ABSTRACT:** We used heparosan (HEP) polysaccharides for controlling nanoparticle delivery to innate immune cells. Our results show that HEP-coated nanoparticles were endocytosed in a time-dependent manner by innate immune cells via both clathrin-mediated and macropinocytosis pathways. Upon endocytosis, we observed HEP-coated nanoparticles in intracellular vesicles and the cytoplasm, demonstrating the potential for nanoparticle escape from intracellular vesicles. Competition with other glycosaminoglycan types inhibited the endocytosis of HEP-coated nanoparticles only partially. We further found that nanoparticle uptake into innate immune cells can be controlled by more than 3 orders of magnitude via systematically varying the HEP surface density. Our results suggest a substantial potential for HEP-coated nanoparticles to target innate immune cells for efficient intracellular delivery, including into the cytoplasm. This HEP nanoparticle surface engineering technology may be broadly used to develop efficient nanoscale devices for drug and gene delivery as well as possibly for gene editing and immuno-engineering applications.

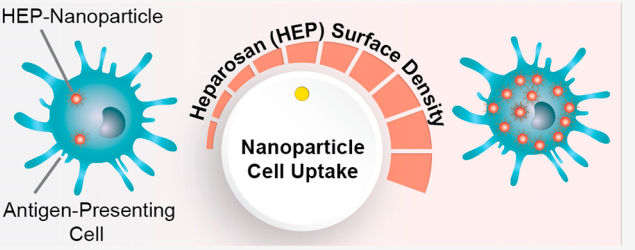


**KEYWORDS:** *Heparosan, surface modification, endocytosis, nanoparticles, antigen-presenting cells, immuno-engineering*

Nanoparticles can deliver biomolecular and other payloads to cells of the innate immune system.[1−3] Upon entry into the body, antigen-presenting cells of the innate immune system can recognize foreign entities, such as pathogens, to elicit immune responses.[3−6] In addition, immune responses can be initiated and boosted through interactions between engineered nanoparticles and immune cells to bridge the gap between innate and adaptive immune systems.[7−11] Therefore, understanding the nanoparticles' interactions with the innate immune system is critical for developing safe and effective nanoparticle-based immunotherapeutics.

In the past decade, multiple nanoparticle surface engineering strategies have been used to target cells of the innate immune system.[5,12−14] However, the observed levels of nanoparticle uptake are not always appropriate for clinical use and may cause cellular or systemic toxicity.[15,16] There is a need to develop methods to control nanoparticle uptake into innate immune cells to elicit desired immune responses.[8,13,17−20] This approach can minimize undesirable side effects of nanomedicines, enabling the development of new nanoparticle-based applications for immunomodulation, immunotherapy, and vaccination.[8,13,17−20]

We demonstrated that heparosan (HEP) is an effective surface engineering technology to create nanoparticles that exhibit reduced protein corona formation with favorable interactions with antigen-presenting cells.[13] This study investigated the interactions between HEP-modified nanoparticles and innate immune cells mechanistically by determining the nanoparticle cellular uptake characteristics and associated endocytosis pathways. Considering that nanoparticle surface properties govern cellular interactions,[15,16,21−23] we investigated the nanoparticle uptake efficiency using competition assays of various HEP structural analogs (i.e., polymers of the glycosaminoglycan (GAG) family) and by systematically varying the HEP surface coating density. Our results show that nanoparticle uptake in innate immune cells can be controlled over 3 orders of magnitude by varying the HEP surface coating density. These findings may enable the development of safe and effective nanomedicines for applications in immuno-engineering, immunotherapy, and vaccine research.

**Received:** June 2, 2022
**Revised:** August 23, 2022

In Figure S1, we demonstrated that HEP-coated gold nanoparticles (HEP-AuNPs) efficiently target antigen-presenting cells, such as macrophages and dendritic cells, consistent with our previous findings.[13] This study used RAW 264.7 macrophages and DC 2.4 dendritic cells as model immune cells. As shown by the light micrographs in Figures 1A and S2, HEP-AuNPs exhibit a time-dependent nanoparticle uptake behavior when incubated with RAW 264.7 macrophages or DC 2.4 dendritic cells. The progressively darker cell coloration (due to the accumulation of AuNPs) upon brightfield imaging over time suggests an increase in nanoparticle uptake. We quantified the nanoparticle cellular uptake in RAW 264.7 (Figure 1B) and DC 2.4 (Figure S3) cells by inductively coupled plasma mass spectrometry (ICP-MS). We observed that the nanoparticle uptake per cell increased over time, plateauing at ~12 h postincubation. These results show that innate immune cells exhibit a time-dependent cellular uptake process to internalize HEP-coated nanoparticles.

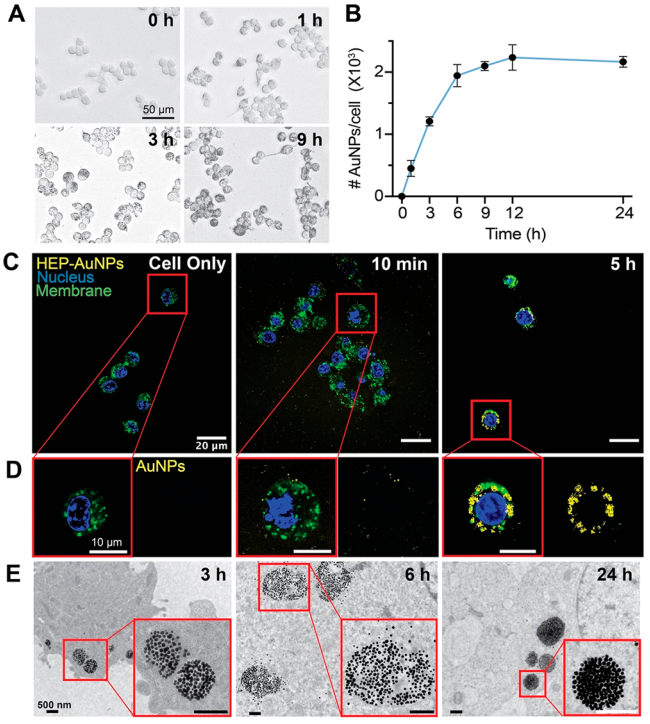


**Figure 1.** The cellular uptake of heparosan (HEP) modified gold nanoparticles (AuNPs) is time-dependent. (A) Representative bright-field light micrographs of HEP-AuNPs internalization in RAW 264.7 macrophages at 0, 1, 3, and 9 h. Scale bar: 50 $\mu$m. (B) ICP-MS results of 55 nm HEP-AuNPs uptake in RAW 264.7 macrophages over time. The data points indicate mean values and standard deviation ($n = 3-4$). (C) Real-time confocal laser scanning microscopy (CLSM) imaging of HEP-AuNP internalization in live RAW 264.7 macrophages. Scale bars: 20 $\mu$m. (D) A representative individual cell image was selected from panel C. The right panel shows the corresponding AuNPs channel. Scale bars: 10 $\mu$m. (E) Transmission electron micrographs of 55 nm HEP-AuNP internalization in RAW 264.7 after 3, 6, and 24 h incubation. The insert at the bottom right corner of each micrograph shows a higher-magnification view of the selected field of view sections. Scale bars: 500 nm.

To further validate the time-dependent cellular internalization, we performed confocal laser scanning microscopy (CLSM) to monitor the nanoparticle uptake behavior in real-time in RAW 264.7 macrophages up to 7 h post-incubation (Figure 1C,D; Figure S4). The HEP-AuNPs were imaged label-free via nanoparticle light scattering and were mainly present surrounding the cell membrane after 1 h of incubation.[13,24] We observed strong intracellular nanoparticle signals at 4.5, 5, and 7 h time points post-incubation. To corroborate the intracellular localization, we subsequently visualized the spatial distribution of nanoparticles in RAW 264.7 macrophages at 3, 6, and 24 h (Figure 1E and Figure S5) and DC 2.4 dendritic cells at 3 and 24 h (Figure S6) post-incubation by transmission electron microscopy (TEM). We observed that the HEP-AuNPs were present in intracellular vesicles and discovered that some nanoparticles could escape from these intracellular vesicles to access the cytoplasm (Figure 1E and S7). Furthermore, we detected some HEP-nanoparticles in lysosomes after 3 h incubation by CLSM via a LysoTracker Deep Red staining, a red fluorescent dye that accumulates in lysosomes (Figure S8). Our findings reveal that the cellular uptake of HEP-AuNPs in RAW 264.7 macrophages and DC 2.4 dendritic cells is time-dependent, with a majority of internalized nanoparticles present in intracellular vesicles and a smaller fraction of nanoparticles accessing the cytoplasm.

Since we observed HEP-AuNPs in intracellular vesicles, we hypothesized that these nanoparticles might enter cells via endocytosis by one or more energy-dependent uptake pathways.[25,26] We carried out a systematic endocytosis inhibition study to discern which uptake pathways were involved (Figure 2A). First, we confirmed that energy-dependent endocytosis facilitated the observed nanoparticle uptake by exposing the RAW 264.7 macrophages to known nonspecific endocytosis inhibition conditions (i.e., low temperature (4 °C) or 0.1% w/v sodium azide).[27−29] We found that the cellular uptake of HEP-AuNPs was reduced by ~89% and ~22% when the cells were incubated with nanoparticles at 4 °C (Figure 2B and Figure S9) or treated with sodium azide, respectively (Figure 2C and Figure S9), confirming an energy-dependent nanoparticle uptake process.

Next, we screened specific endocytosis pathways using established chemical inhibitors (Table 1) that more selectively block endocytosis using inhibitor concentrations from the literature (Figure 2A). First, we pre-incubated the innate immune cells for 1 h with the endocytosis inhibitors. Then we added the nanoparticles and incubated them with the cells for 1.5 h. We imaged the cells with a light microscope and quantified the nanoparticle uptake by ICP-MS (Figure 2D and Figures S9−S10). The ICP-MS results revealed that nanoparticle cellular uptake inhibition efficiencies were ~73%, 12%, 24%, or 8% for chlorpromazine, chloroquine, cytochalasin D, or imipramine, respectively (Figure 2D).

Under our study conditions, the chlorpromazine inhibitor was the most effective agent. As shown in Figures 2D and S9−S10, the endocytosis inhibitors N-ethylmaleimide (NEM), filipin, dynasore, and 5-(*N*-ethyl-*N*-isopropyl) amiloride (EIPA) did not reduce the nanoparticle cellular uptake. It is known that the cellular uptake machinery and cellular metabolic processes are interconnected, and thus, uptake and transport mechanisms in the context of nanoparticles are difficult to completely define.[30] However, our findings suggest that HEP-AuNPs primarily enter the model innate immune cells through clathrin-mediated endocytosis and macropinocytosis pathways with some possibility of phagocytosis.

As schematically shown in Figure 3A, chlorpromazine inhibits clathrin-mediated endocytosis while cytochalasin D inhibits macropinocytosis/phagocytosis.[51,53] In our screening experi-


https://doi.org/10.1021/acs.nanolett.2c02226
Nano Lett. XXXX, XXX, XXX−XXX

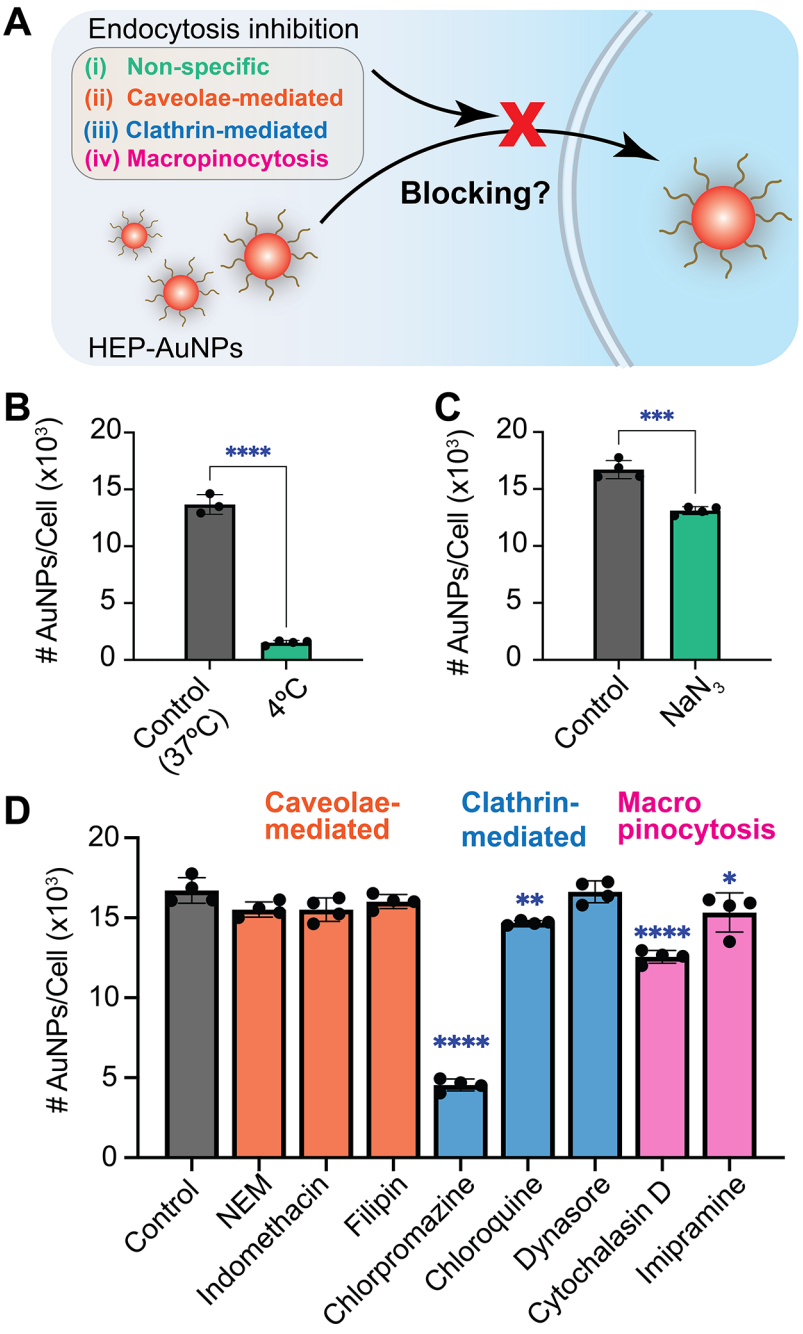


**Figure 2.** HEP-coated nanoparticles enter innate immune cells through endocytosis. (A) Schematic representation of the uptake pathway study: (i) nonspecific endocytosis inhibition to determine whether nanoparticle cellular uptake is energy-dependent. (ii–iv) Specific endocytosis inhibitors for studying (ii) caveolae-mediated endocytosis, (iii) clathrin-mediated endocytosis, and (iv) macropinocytosis. (B–D) ICP-MS quantification of the nanoparticle cellular uptake in RAW 264.7 macrophages at 4 °C (B), in the presence of ATPase inhibitor sodium azide (C), or chemical endocytosis inhibitors of caveolae-mediated endocytosis, clathrin-mediated endocytosis, and macropinocytosis (D). AuNPs modified with 13-kDa HEP (at 0.2 nM) were used as control without inhibitors at 37 °C. Bars indicate mean ± SD ($n$ = 3–4); statistical tests used one-way ANOVA ($p$ < 0.0001 (****); $p$ < 0.0021 (**); $p$ < 0.0332 (*).

ments, these agents were the most effective HEP-AuNP uptake inhibitors (Figure 2). We performed systematic dose escalation studies to assess the dose–response of the inhibitory effect and the cell toxicity of these two agents. Based on the previous dose screening experiments and published cell viability data,[30,54,55] the dose ranges were 0–31.4 $\mu$M and 0–3.9 $\mu$M for chlorpromazine and cytochalasin D, respectively. The cell viability assays confirmed that these inhibitor doses were not cytotoxic under the tested conditions (Figure 3B,C). Using ICP-MS analysis, we quantified the inhibitory effects for nanoparticle uptake in RAW264.7 macrophages to be ~70% (chlorpromazine) and ~51% (cytochalasin D), respectively (Figure 3B,C). Furthermore, the cell light micrographs showed an apparent reduction in light extinction, consistent with a decrease in nanoparticle cellular uptake (Figures S11–S12). The notably reduced cellular uptake levels upon chlorpromazine (23.5 $\mu$M) and Cytochalasin D (3.0 $\mu$M) incubation with RAW 264.7 macrophages were confirmed qualitatively by CLSM imaging (Figure 3D). Reduced nanoparticle intensity signals were


https://doi.org/10.1021/acs.nanolett.2c02226
Nano Lett. XXXX, XXX, XXX–XXX

**Table 1. Summary of Endocytosis Inhibition Conditions Used in This Study**

| inhibitor | mechanism of action[a] | function/pathway[a] | condition/ concentration | ref |
|---|---|---|---|---|
| low temperature | lowers metabolism | nonspecific endocytosis | 4 °C | 27 |
| sodium azide ($NaN_3$) | decreases ATP by inhibiting glycolysis | nonspecific endocytosis | 0.1% w/v | 31 |
| *N*-ethylmaleimide (NEM) | inactivates the ATPase | caveolae-mediated endocytosis | 0.3 μg/mL | 32−34 |
| indomethacin | increases [arachidonate] to prevent plasmalemmal vesicle formation | caveolae-mediated and clathrin-dependent endocytosis | 10 μg/mL | 35 |
| filipin | removes cholesterol from the plasma membrane | caveolae-mediated and clathrin-independent endocytosis | 5 μg/mL | 36 |
| chlorpromazine (CPZ) | unknown (AP2 inhibition?) | clathrin-mediated endocytosis | 10 μg/mL | 35,36 |
| chloroquine | Rho GTPase inhibition | clathrin-mediated endocytosis | 30 μg/mL | 37 |
| dynasore | blocks GTPase activity of dynamin | clathrin-mediated endocytosis | 25 μg/mL | 38 |
| cytochalasin D (CD) | depolymerizes F-actin | macropinocytosis and phagocytosis | 1 μg/mL | 38,39 |
| imipramine | inhibits the ruffling of plasma membranes | macropinocytosis | 10 μg/mL | 40 |
| amiloride (EIPA) | inhibits $Na^+$ channels and $Na^+/H^+$ exchange, F-action reorganization, pseudopodia retraction | macropinocytosis and phagocytosis | 10 or 20 μg/mL | 41 |
| Cdc42/Rac1 | inhibits Cdc42 and Rac1 involved regulation of actin cytoskeleton organization | phagocytosis | 1.2−40 μg/mL | 42,43 |
| NSC23766 | inhibits the activity of Rac1 | phagocytosis | 1.6−106 μg/mL | 44−46 |
| 3-μm polymeric microspheres | saturation of phagocytosis capacity | phagocytosis | microsphere to cell ratio of 20:1 | 47 |
| annexin V | masks exposed phosphatidylserine | phagocytosis | 750 μg/mL | 48−50 |

[a]Information on the mechanisms of action and functions/pathways was adopted in part from reviews by Sheth et al., Rennick et al., and Almeida et al.[41,51,52]

**Table 2. Summary of HEP Structural Analog Polymers Used for Competition Experiments in This Study**

| GAG* or sugar | average molecular weight (kDa) | surface receptors (not all inclusive) | major repeat structure | similarity with heparosan | difference from heparosan | ref |
|---|---|---|---|---|---|---|
| heparosan | 43.8; 169 | | [GlcA]-4-beta-[GlcNAc]-4-alpha | - | - | |
| hyaluronic acid (HA) | 160; 1000 | CD 44; LYVE-1; HARE; stabilin-1 | [GlcA]-3-beta-[GlcNAc]-4-beta | same sugar composition and charge density | different glycosidic linkages | 56−58 |
| heparan sulfate | ∼12.9 | fibroblast growth factor receptor | [GlcA]-[6OS-GlcNAc/ GlcNS] | same backbone | ∼1−2 sulfates per repeat | 59,60 |
| heparin | ∼16.6 | G6b; fibroblast growth factor receptor; FGF2 | [2S-IdoA/GlcA]-[6OS-GlcNS] | similar backbone | ∼3 sulfates per repeat; some GlcA epimer, IdoA | 58,59,61,62 |
| chondroitin sulfate A (CS A) | ∼19.5 | CD 44 | [GlcA]-3-beta-[4S-GalNAc]-4-beta | GAG family | GalNAc instead of GlcNAc; different glycosidic linkages; 1 sulfate per repeat | 59,60,63−65 |
| chondroitin sulfate B (CS B) | ∼21 | | [2S-GlcA/IdoA]-3-beta-[4,6S-GalNAc]-4-beta | GAG family | GalNAc instead of GlcNAc; different glycosidic linkages; ∼2 sulfates per repeat | 66 |
| chondroitin sulfate C (CS C) | ∼45 | CD 44 | [GlcA]-3-beta-[6S-GalNAc]-4-beta | GAG family | GalNAc instead of GlcNAc; different glycosidic linkages; 1 sulfate per repeat | 2 |
| chondroitin sulfate D (CS D) | ∼39 | | [2S-GlcA]-3-beta-[6S-GalNAc]-4-beta | GAG family | GalNAc instead of GlcNAc; different glycosidic linkages; ∼2 sulfates per repeat | 67 |
| chondroitin sulfate E (CS E) | ∼140 | contactin-1 | [GlcA]-3-beta-[4,6S-GalNAc]-4-beta | GAG family | GalNAc instead of GlcNAc; different glycosidic linkages; ∼2 sulfates per repeat | 67,68 |
| unsulfated chondroitin | ∼100−200 | | [GlcA]-3-beta-[GalNAc]-4-beta | GAG family; same charge density | GalNAc instead of GlcNAc | |
| GlcNAc (*N*-acetyl-glucosamine) | 0.221 | - | - | monosaccharide component | - | 69 |

*GAG: glycosaminoglycan.

observed in the cell groups treated with the inhibitors compared to those without the inhibitors (Figure 3D).

To test whether the HEP-coated nanoparticles could enter cells through clathrin-mediated endocytosis and macropinocytosis/phagocytosis in another immune cell line, we conducted similar inhibition experiments in DC 2.4 dendritic cells. As shown in Figure S13, both chlorpromazine and cytochalasin D reduced HEP-AuNP uptake by ∼77% in DC 2.4 dendritic cells.



https://doi.org/10.1021/acs.nanolett.2c02226
Nano Lett. XXXX, XXX, XXX−XXX

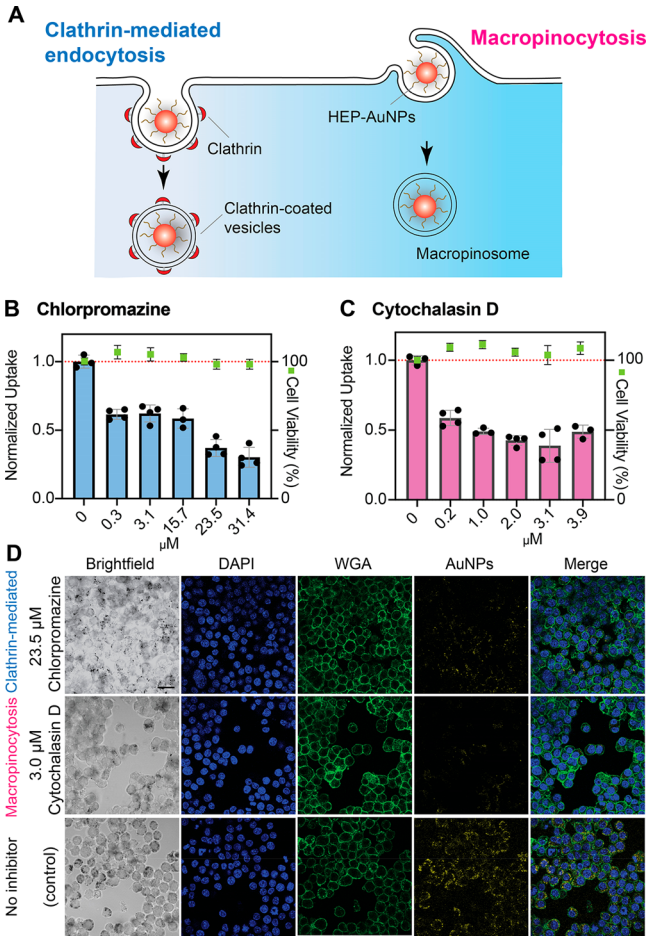


**Figure 3.** HEP-coated nanoparticles enter cells primarily through clathrin-mediated endocytosis and macropinocytosis. (A) Schematic representation of HEP-AuNPs uptake through clathrin-mediated endocytosis or macropinocytosis. (B,C) ICP-MS was used to quantify the nanoparticle cellular uptake in RAW 264.7 macrophages upon endocytosis inhibition with different concentrations of chlorpromazine (B; clathrin-mediated endocytosis) and cytochalasin D (C; macropinocytosis), respectively. Bars indicate mean values ± SD ($n$ = 3−4). The statistical analysis of groups with competitors showed $p < 0.0001$ compared to the no-competitor group using one-way ANOVA. (D) Confocal laser scanning micrographs of nanoparticle uptake in the presence of endocytosis inhibitors chlorpromazine or cytochalasin D along with non-inhibition control. Scale bar: 20 $\mu$m.

Additionally, we co-incubated chlorpromazine and cytochalasin D inhibitors with cells to test if there was any additive endocytosis inhibitory effect. Upon co-incubation of these two inhibitors, we quantified an ∼71% inhibitory effect. Thus, significant additive endocytosis inhibition was not observed with this inhibitor combination. We corroborated this finding by co-incubating RAW 264.7 macrophages with both inhibitors (Figure S14). We observed no significant cytotoxicity of the inhibitors at these tested doses (Figure S15).

To investigate the role of phagocytosis on the HEP-AuNPs cellular uptake, we conducted a systematic set of experiments involving inhibition of the process via: (i) physical saturation with 3-$\mu$m polymeric microspheres and (ii) chemical inhibition by the compounds Cdc42/Rac1 and NSC 23766 (Table 1) in RAW 264.7 and DC 2.4 cells. As shown in Figures S16−S19, there was no significant reduction of HEP-nanoparticle cellular uptake suggesting only a potentially minor role of phagocytosis.

We additionally did not observe an inhibitory effect on nanoparticle cellular uptake in RAW 264.7 upon using annexin V as a potential phagocytosis competitor/inhibitor (Table 1, Figure S20). Our results indicate that the cell uptake of HEP-AuNPs occurs in a time-dependent manner facilitated primarily by clathrin-mediated endocytosis and macropinocytosis.

Our experiments showed that clathrin-mediated endocytosis plays an important role in the cellular uptake of HEP-AuNPs, indicating that specific cell surface receptors may facilitate nanoparticle cell uptake. Since these cell surface receptors are unknown, we wondered whether various structural analogs of HEP polysaccharides, the glycosaminoglycans (GAGs) including heparin, hyaluronan (HA), chondroitin sulfates (CS), could be used as competitors and thereby reduce the uptake of HEP-AuNPs (Figure 4A).

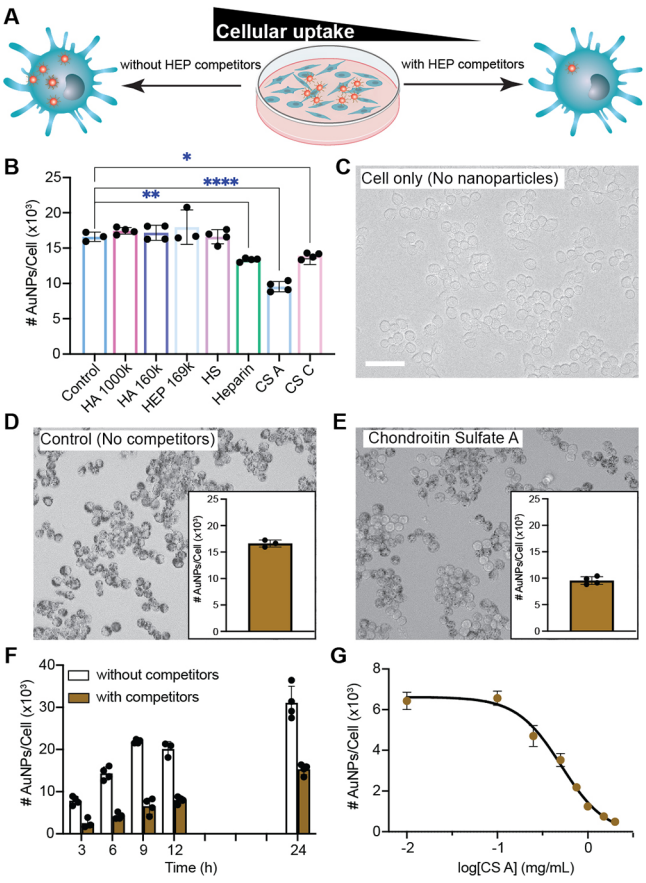


**Figure 4.** Evaluation of structural HEP analog polymers as competitors for HEP-coated nanoparticle uptake. (A) Schematic illustration of the experimental design. (B) ICP-MS was used to quantify the cellular uptake of HEP-AuNPs in the presence of HEP structural analogs: 0.1 mg/mL 1,000-kDa HA, 160-kDa HA, 169-kDa HEP, heparin sulfate (HS), or heparin, and 1 mg/mL chondroitin sulfate A (CS A) or chondroitin sulfate C (CS C). The bars indicate mean values ± SD ($n$ = 3−4). Statistical tests were performed using one-way ANOVA ($p < 0.0001$ (****); $p < 0.0021$ (**); $p < 0.0332$ (*); n.s. indicates no statistically significant differences). (C−E) Representative brightfield light micrographs of HEP-AuNPs cell uptake in the presence of competitors. The inserted bar graphs represent the quantitative ICP-MS results. The bars indicate mean values ± SD ($n$ = 3−4). Scale bar: 50 $\mu$m. (F,G) ICP-MS was used to quantify the CS A competition efficiency to reduce HEP-AuNPs cellular uptake over time (F; 1 mg/mL CS A was used) and various CS A concentrations (G). The graphs indicate mean values ± SD ($n$ = 3−4).


https://doi.org/10.1021/acs.nanolett.2c02226
Nano Lett. XXXX, XXX, XXX−XXX

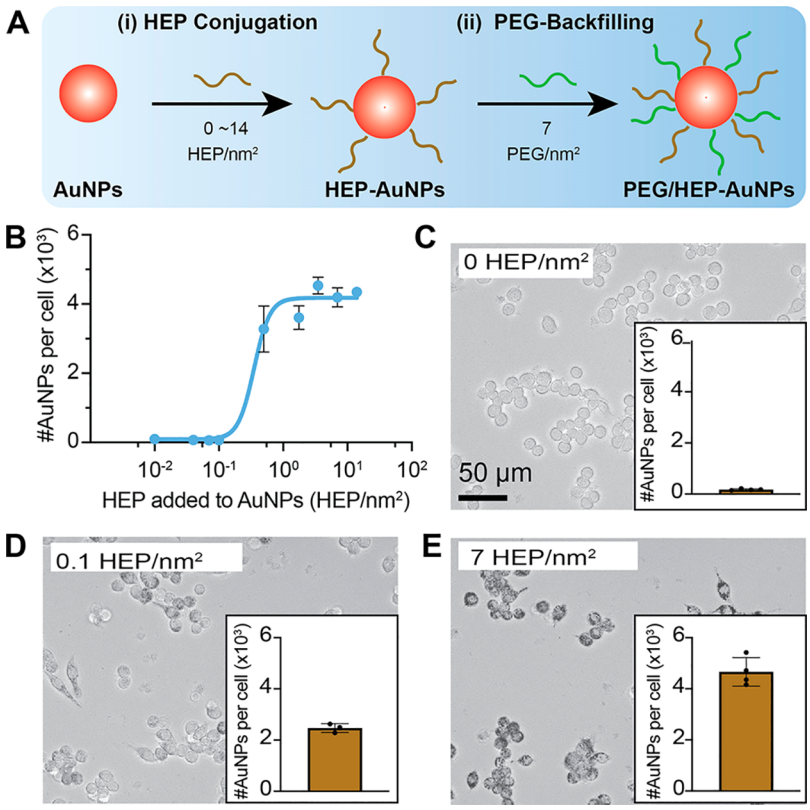


**Figure 5.** Nanoparticle surface coating with HEP promotes multivalent interactions with innate immune cells. (A) Schematic representation of the surface coating process. (i) The HEP polymers were added to the AuNPs with theoretical surface coating densities ranging from 0 to 14 HEP/nm$^2$ added to the preparations. (ii) Backfilling of the nanoparticle surface was achieved by adding a constant saturating amount of PEG (adding the equivalent of 7 PEG/nm$^2$ to the preparations) to generate HEP/PEG-AuNPs. (B) The uptake efficiency was measured as a function of the added surface HEP density by ICP-MS. The data points indicate mean values ± SD ($n$ = 3−4). (C−E) Representative brightfield light micrographs of HEP/PEG-AuNPs in cells. The dark colorations within the cells indicate nanoparticle accumulation. The inserted bar graphs display the quantitative ICP-MS results of nanoparticle cell uptake. The data points indicate mean values ± SD ($n$ = 3−4). Scale bar: 50 $\mu$m.

To address this question, we pre-incubated RAW 264.7 macrophages systematically with a library of relevant HEP structural analogs (Table 2) and then added HEP-AuNPs to the cells. To quantify the nanoparticles' cellular interactions, we performed quantitative ICP-MS (Figure 4B and Figures S21−S22) and corroborated the results qualitatively with light microscopy (Figure 4C−E, Figures S23−S25). The ICP-MS and microscopy data both revealed that CS A (i.e., CS with mostly C4-sulfo isomers) was most effective at reducing the cellular uptake (~43%) of HEP-AuNPs compared with the "no-competitors" group. We observed ~15% inhibition by CS C (i.e., CS with mostly C6-sulfo isomers) and ~18% inhibition by heparin (i.e., the anticoagulant drug that is a highly sulfated HEP); no significant competition with the remaining structural analogs was observed (Figure 4B, Figures S21−S22). Heparosan itself was not a good competitor (either the high molecular weight 169-kDa HEP or the 13-kDa HEP used for the nanoparticle coating). We speculate that the multivalent interactions of the HEP-AuNPs with cells were too strong to be effectively competed by a "monovalent" free HEP chain.

We next investigated whether the observed CS A inhibition of HEP-AuNP uptake was due to a potential toxicity effect of the CS A preparation, which was extracted from a mammalian source. We observed that the CS A material did not affect cell viability at the working concentrations employed in this study (Figures 4C−E, S21, S23−S25).

Next, we expanded the structural analog competition study to DC 2.4 dendritic cells. Since the previous study demonstrated that CS A significantly reduced uptake of the HEP-AuNPs in RAW 264.7 macrophages, we pre-incubated CS A with the DC 2.4 cells for 1 h, then added the nanoparticles for an additional 2.5-h incubation. We quantified the competition efficiency by ICP-MS and corroborated the results with light microscopy (Figures S25−S26). Non-cytotoxic doses of CS A resulted in a lower nanoparticle uptake as quantified by ICP-MS, and we observed a reduced nanoparticle signal compared to the no-competitors group using light microscopy (Figures S25−S26).

We further assessed the competition effect of CS A as a function of time and concentration at non-cytotoxic levels. The CS A agent significantly lowered the cell uptake of HEP-AuNPs, as confirmed by light microscopy and ICP-MS quantification (Figures S27−S30 and Figures 4F,G). The inhibitory effect of 1 mg/mL CS A persisted throughout time (Figure 4F). At 2 mg/mL, CS A suppressed cellular uptake of HEP-AuNPs up to 9-fold, according to our inhibitor dose−response results ($IC_{50}$ of 0.5 mg/mL, Figure 4G). These competition experiments with GAG structural analog polymers imply that CS A can substitute as a ligand for HEP for the internalization receptor(s). However, the receptor identity remains unknown.

Next, we investigated whether the observed substantial cellular uptake of HEP-AuNPs was due to multivalent nanoparticle/receptor interactions by evaluating the effect of the HEP surface coating density on internalization. Since


https://doi.org/10.1021/acs.nanolett.2c02226
Nano Lett. XXXX, XXX, XXX−XXX

uncoated nanoparticles are prone to colloidal instability and substantial protein corona formation that may affect cellular interactions,[70−75] we first coated the nanoparticles with various amounts of HEP polymers. We then used a backfilling strategy to cover any uncoated surface with methoxy-terminated poly(ethylene glycol), PEG, thereby enhancing nanoparticle colloidal stability (Figure 5A and Figure S1). PEG is known to minimize nonspecific protein adsorption on nanoparticle surfaces, and it is used in the clinic.[13,76] We characterized the coating process by measuring the hydrodynamic diameter and zeta potential with DLS. The data show that with HEP added at ≥0.5 HEP/nm$^2$, there was no significant difference in the hydrodynamic diameter or the zeta potential values after PEG backfilling. At the added densities of <0.5 HEP/nm$^2$, the hydrodynamic diameter and the zeta potential increased with the addition of PEG, indicating that the nanoparticles were successfully backfilled (Figures S31 and S32A,B). These results confirm that fully surface-coated nanoparticles with various HEP densities were generated successfully.

Next, we exposed the nanoparticles with various HEP surface coating densities to RAW 264.7 macrophages and evaluated the corresponding uptake efficiencies qualitatively by light microscopy and quantitatively by ICP-MS (Figure 5B−E and Figure S32C,D). We observed that the interaction between the nanoparticles and the cells increased in a HEP surface coating density-dependent manner using light microscopy (Figure 5C−E and Figures S32D−S33). We corroborated this observation quantitatively by ICP-MS. Our quantitative results demonstrate that the nanoparticle cellular uptake can be controlled by more than 3 orders of magnitude via varying the HEP surface coating density (Figure 5B and Figure S32C). Overall, our results suggest that the multivalent interactions strengthen with increased HEP surface coating density, leading to higher HEP-AuNP cell uptake. Manipulating the surface HEP coating density could provide a strategy for the controlled delivery of nanoparticles to innate immune cells.

In the current work, we studied the cellular uptake behavior and endocytosis pathways of HEP-AuNPs in innate immune cells (e.g., macrophages and dendritic cells) that are antigen-presenting cells. Our results demonstrate that HEP-coated nanoparticles are endocytosed by cells in a time-dependent manner and internalized into intracellular vesicles through clathrin-mediated endocytosis and macropinocytosis. We found that some fraction of internalized nanoparticles could access the cytoplasm potentially via endosomal escape. The nanoparticle cellular uptake is strongly affected by the HEP surface coating density. This nanoparticle uptake can be controlled over 3 orders of magnitude through HEP surface coating density engineering. The ability to control the uptake of HEP-coated nanoparticles in innate immune cells could enable the future development of safe, effective, and efficient nanoparticle-based immunotherapies and vaccines.

## ■ ASSOCIATED CONTENT

### Supporting Information

The Supporting Information is available free of charge at https://pubs.acs.org/doi/10.1021/acs.nanolett.2c02226.

Supplementary figures S1−S33 and the methods and materials (PDF)

## ■ AUTHOR INFORMATION


### Corresponding Author

**Stefan Wilhelm** − *Stephenson School of Biomedical Engineering, University of Oklahoma, Norman, Oklahoma 73019, United States; Stephenson Cancer Center, University of Oklahoma Health Sciences Center, Oklahoma City, Oklahoma 73104, United States; Institute for Biomedical Engineering, Science, and Technology (IBEST), University of Oklahoma, Norman, Oklahoma 73019, United States;* orcid.org/0000-0003-2167-6221; Email: stefan.wilhelm@ou.edu

### Authors

**Wen Yang** − *Stephenson School of Biomedical Engineering, University of Oklahoma, Norman, Oklahoma 73019, United States*

**Alex N. Frickenstein** − *Stephenson School of Biomedical Engineering, University of Oklahoma, Norman, Oklahoma 73019, United States*

**Vinit Sheth** − *Stephenson School of Biomedical Engineering, University of Oklahoma, Norman, Oklahoma 73019, United States*

**Alyssa Holden** − *Stephenson School of Biomedical Engineering, University of Oklahoma, Norman, Oklahoma 73019, United States*

**Evan M. Mettenbrink** − *Stephenson School of Biomedical Engineering, University of Oklahoma, Norman, Oklahoma 73019, United States*

**Lin Wang** − *Stephenson School of Biomedical Engineering, University of Oklahoma, Norman, Oklahoma 73019, United States;* orcid.org/0000-0003-4636-8225

**Alexis A. Woodward** − *Stephenson School of Biomedical Engineering, University of Oklahoma, Norman, Oklahoma 73019, United States*

**Bryan S. Joo** − *Stephenson School of Biomedical Engineering, University of Oklahoma, Norman, Oklahoma 73019, United States*

**Sarah K. Butterfield** − *Stephenson School of Biomedical Engineering, University of Oklahoma, Norman, Oklahoma 73019, United States*

**Nathan D. Donahue** − *Stephenson School of Biomedical Engineering, University of Oklahoma, Norman, Oklahoma 73019, United States*

**Dixy E. Green** − *Department of Biochemistry and Molecular Biology, University of Oklahoma Health Sciences Center, Oklahoma City, Oklahoma 73104, United States*

**Abigail G. Thomas** − *Stephenson School of Biomedical Engineering, University of Oklahoma, Norman, Oklahoma 73019, United States*

**Tekena Harcourt** − *Stephenson School of Biomedical Engineering, University of Oklahoma, Norman, Oklahoma 73019, United States*

**Hamilton Young** − *Stephenson School of Biomedical Engineering, University of Oklahoma, Norman, Oklahoma 73019, United States;* orcid.org/0000-0003-2249-5780

**Mulan Tang** − *Stephenson School of Biomedical Engineering, University of Oklahoma, Norman, Oklahoma 73019, United States*

**Zain A. Malik** − *Stephenson School of Biomedical Engineering, University of Oklahoma, Norman, Oklahoma 73019, United States*

**Roger G. Harrison** − *School of Chemical, Biological and Materials Engineering, University of Oklahoma, Norman,*




https://doi.org/10.1021/acs.nanolett.2c02226
Nano Lett. XXXX, XXX, XXX−XXX

*Oklahoma 73019, United States;* orcid.org/0000-0003-2401-627X

**Priyabrata Mukherjee** − *Department of Pathology, The University of Oklahoma Health Sciences Center, Oklahoma City, Oklahoma 73104, United States; Stephenson Cancer Center, University of Oklahoma Health Sciences Center, Oklahoma City, Oklahoma 73104, United States;* orcid.org/0000-0002-0557-0833

**Paul L. DeAngelis** − *Department of Biochemistry and Molecular Biology, University of Oklahoma Health Sciences Center, Oklahoma City, Oklahoma 73104, United States*

Complete contact information is available at: https://pubs.acs.org/10.1021/acs.nanolett.2c02226

### Notes

The authors declare no competing financial interest.

## ■ ACKNOWLEDGMENTS

The authors thank Dr. Chen for providing the DC 2.4 dendritic cells. Additionally, the authors acknowledge the University of Oklahoma (OU) Samuel Roberts Noble Microscopy Laboratory (SRNML), the OU Mass Spectrometry, Proteomics & Metabolomics (MSPM) Core, and the Oklahoma Medical Research Foundation (OMRF) Imaging Core Facility for assistance. This work was supported in part by an NSF MRI grant (1828234), NSF CAREER award (2048130), an NIH COBRE award (P20GM135009), an IBEST/OUHSC seed grant for interdisciplinary research, the OU VPRP Strategic Equipment Investment grant, the OU Faculty Investment Program, an OCAST Health Research grant (HR20-106), Oklahoma Center for the Advancement of Science and Technology, and the Oklahoma Tobacco Settlement Endowment Trust awarded to the University of Oklahoma Stephenson Cancer Center. The content is solely the responsibility of the authors and does not necessarily represent the official views of the Oklahoma Tobacco Settlement Endowment Trust. P.M. acknowledges funding from NIH R01CA136494 and R01CA213278.

## ■ REFERENCES

(1) Wilhelm, S.; Tavares, A. J.; Dai, Q.; Ohta, S.; Audet, J.; Dvorak, H. F.; Chan, W. C. W. Analysis of Nanoparticle Delivery to Tumours. *Nat. Rev. Mater.* **2016**, *1* (5), 1−12.

(2) Zhao, Z.; Ukidve, A.; Kim, J.; Mitragotri, S. Targeting Strategies for Tissue-Specific Drug Delivery. *Cell* **2020**, *181* (1), 151−167.

(3) Boraschi, D.; Italiani, P.; Palomba, R.; Decuzzi, P.; Duschl, A.; Fadeel, B.; Moghimi, S. M. Nanoparticles and Innate Immunity: New Perspectives on Host Defence. *Seminars in Immunology* **2017**, *34*, 33−51.

(4) Aroh, C.; Wang, Z.; Dobbs, N.; Luo, M.; Chen, Z.; Gao, J.; Yan, N. Innate Immune Activation by CGAMP-PC7A Nanoparticles Leads to Potent and Long-Acting Antiretroviral Response against HIV-1. *J. Immunol* **2017**, *199* (11), 3840−3848.

(5) Liu, Y.; Hardie, J.; Zhang, X.; Rotello, V. M. Effects of Engineered Nanoparticles on the Innate Immune System. *Semin Immunol* **2017**, *34*, 25−32.

(6) La-Beck, N. M.; Gabizon, A. A. Nanoparticle Interactions with the Immune System: Clinical Implications for Liposome-Based Cancer Chemotherapy. *Frontiers in Immunology* **2017**, *8*, 416.

(7) Donahue, N. D.; Acar, H.; Wilhelm, S. Concepts of Nanoparticle Cellular Uptake, Intracellular Trafficking, and Kinetics in Nanomedicine. *Adv. Drug Delivery Rev.* **2019**, *143*, 68−96.

(8) Yang, W.; Wang, L.; Mettenbrink, E. M.; DeAngelis, P. L.; Wilhelm, S. Nanoparticle Toxicology. *Annu. Rev. Pharmacol. Toxicol.* **2021**, *61* (1), 269−289.

(9) Beck, J. D.; Reidenbach, D.; Salomon, N.; Sahin, U.; Türeci, Ö.; Vormehr, M.; Kranz, L. M. MRNA Therapeutics in Cancer Immunotherapy. *Mol. Cancer* **2021**, *20*, 69.

(10) Yin, Q.; Yu, W.; Grzeskowiak, C. L.; Li, J.; Huang, H.; Guo, J.; Chen, L.; Wang, F.; Zhao, F.; von Boehmer, L.; Metzner, T. J.; Leppert, J. T.; Chien, Y.-H.; Kuo, C. J.; Davis, M. M. Nanoparticle-Enabled Innate Immune Stimulation Activates Endogenous Tumor-Infiltrating T Cells with Broad Antigen Specificities. *Proc. Natl. Acad. Sci. U. S. A.* **2021**, *118* (21), No. e2016168118.

(11) Iwasaki, A.; Medzhitov, R. Regulation of Adaptive Immunity by the Innate Immune System. *Science* **2010**, *327* (5963), 291−295.

(12) Mizrahy, S.; Raz, S. R.; Hasgaard, M.; Liu, H.; Soffer-Tsur, N.; Cohen, K.; Dvash, R.; Landsman-Milo, D.; Bremer, M. G. E. G.; Moghimi, S. M.; Peer, D. Hyaluronan-Coated Nanoparticles: The Influence of the Molecular Weight on CD44-Hyaluronan Interactions and on the Immune Response. *J. Controlled Release* **2011**, *156* (2), 231−238.

(13) Yang, W.; Wang, L.; Fang, M.; Sheth, V.; Zhang, Y.; Holden, A. M.; Donahue, N. D.; Green, D. E.; Frickenstein, A. N.; Mettenbrink, E. M.; Schwemley, T. A.; Francek, E. R.; Haddad, M.; Hossen, M. N.; Mukherjee, S.; Wu, S.; DeAngelis, P. L.; Wilhelm, S. Nanoparticle Surface Engineering with Heparosan Polysaccharide Reduces Serum Protein Adsorption and Enhances Cellular Uptake. *Nano Lett.* **2022**, *22* (5), 2103−2111.

(14) Liu, Y.; Wang, L.; Song, Q.; Ali, M.; Crowe, W. N.; Kucera, G. L.; Hawkins, G. A.; Soker, S.; Thomas, K. W.; Miller, L. D.; Lu, Y.; Bellinger, C. R.; Zhang, W.; Habib, A. A.; Petty, W. J.; Zhao, D. Intrapleural Nano-Immunotherapy Promotes Innate and Adaptive Immune Responses to Enhance Anti-PD-L1 Therapy for Malignant Pleural Effusion. *Nat. Nanotechnol* **2022**, *17* (2), 206−216.

(15) Ding, H.; Ma, Y. Controlling Cellular Uptake of Nanoparticles with PH-Sensitive Polymers. *Sci. Rep* **2013**, *3* (1), 2804.

(16) Bai, Y.; Xing, H.; Wu, P.; Feng, X.; Hwang, K.; Lee, J. M.; Phang, X. Y.; Lu, Y.; Zimmerman, S. C. Chemical Control over Cellular Uptake of Organic Nanoparticles by Fine Tuning Surface Functional Groups. *ACS Nano* **2015**, *9* (10), 10227−10236.

(17) Costa da Silva, M.; Vieira Rocha, C.; Bañobre-López, M.; Gallo, J. Stimulation and Suppression of the Innate Immune System through Nanotechnology. *ACS Appl. Nano Mater.* **2021**, *4* (3), 2303−2316.

(18) Cai, J.; Wang, H.; Wang, D.; Li, Y. Improving Cancer Vaccine Efficiency by Nanomedicine. *Adv. Biosys.* **2019**, *3* (3), 1800287.

(19) van Leent, M. M. T.; Priem, B.; Schrijver, D. P.; de Dreu, A.; Hofstraat, S. R. J.; Zwolsman, R.; Beldman, T. J.; Netea, M. G.; Mulder, W. J. M. Regulating Trained Immunity with Nanomedicine. *Nat. Rev. Mater.* **2022**, No. 7, 465−481.

(20) Moynihan, K. D.; Opel, C. F.; Szeto, G. L.; Tzeng, A.; Zhu, E. F.; Engreitz, J. M.; Williams, R. T.; Rakhra, K.; Zhang, M. H.; Rothschilds, A. M.; Kumari, S.; Kelly, R. L.; Kwan, B. H.; Abraham, W.; Hu, K.; Mehta, N. K.; Kauke, M. J.; Suh, H.; Cochran, J. R.; Lauffenburger, D. A.; Wittrup, K. D.; Irvine, D. J. Eradication of Large Established Tumors in Mice by Combination Immunotherapy That Engages Innate and Adaptive Immune Responses. *Nat. Med.* **2016**, *22* (12), 1402−1410.

(21) Verma, A.; Stellacci, F. Effect of Surface Properties on Nanoparticle-Cell Interactions. *Small* **2010**, *6* (1), 12−21.

(22) Nel, A. E.; Mädler, L.; Velegol, D.; Xia, T.; Hoek, E. M. V.; Somasundaran, P.; Klaessig, F.; Castranova, V.; Thompson, M. Understanding Biophysicochemical Interactions at the Nano-Bio Interface. *Nat. Mater.* **2009**, *8* (7), 543−557.

(23) Chou, L. Y. T.; Ming, K.; Chan, W. C. W. Strategies for the Intracellular Delivery of Nanoparticles. *Chem. Soc. Rev.* **2011**, *40* (1), 233−245.

(24) Donahue, N. D.; Sheth, V.; Frickenstein, A. N.; Holden, A.; Kanapilly, S.; Stephan, C.; Wilhelm, S. Absolute Quantification of Nanoparticle Interactions with Individual Human B Cells by Single Cell Mass Spectrometry. *Nano Lett.* **2022**, *22* (10), 4192−4199.

(25) Fobian, S.-F.; Petzer, M.; Vetten, M.; Steenkamp, V.; Gulumian, M.; Cordier, W. Mechanisms Facilitating the Uptake of Carboxyl-Polythene Glycol-Functionalized Gold Nanoparticles into Multicellular Spheroids. *J. Pharm. Pharmacol.* **2022**, rgac017.
(26) Foroozandeh, P.; Aziz, A. A. Insight into Cellular Uptake and Intracellular Trafficking of Nanoparticles. *Nanoscale Res. Lett.* **2018**, *13* (1), 339.
(27) Li, Y.; Monteiro-Riviere, N. A. Mechanisms of Cell Uptake, Inflammatory Potential and Protein Corona Effects with Gold Nanoparticles. *Nanomedicine* **2016**, *11* (24), 3185−3203.
(28) Gao, H.; Yang, Z.; Zhang, S.; Cao, S.; Shen, S.; Pang, Z.; Jiang, X. Ligand Modified Nanoparticles Increases Cell Uptake, Alters Endocytosis and Elevates Glioma Distribution and Internalization. *Sci. Rep* **2013**, *3*, 2534.
(29) Kou, L.; Sun, J.; Zhai, Y.; He, Z. The Endocytosis and Intracellular Fate of Nanomedicines: Implication for Rational Design. *Asian Journal of Pharmaceutical Sciences* **2013**, *8* (1), 1−10.
(30) Francia, V.; Reker-Smit, C.; Boel, G.; Salvati, A. Limits and Challenges in Using Transport Inhibitors to Characterize How Nano-Sized Drug Carriers Enter Cells. *Nanomedicine* **2019**, *14* (12), 1533−1549.
(31) Reisman, B. J.; Guo, H.; Ramsey, H. E.; Wright, M. T.; Reinfeld, B. I.; Ferrell, P. B.; Sulikowski, G. A.; Rathmell, W. K.; Savona, M. R.; Plate, L.; Rubinstein, J. L.; Bachmann, B. O. Apoptolidin Family Glycomacrolides Target Leukemia through Inhibition of ATP Synthase. *Nat. Chem. Biol.* **2022**, *18* (4), 360−367.
(32) Delrot, S.; Despeghel, J.-P.; Bonnemain, J.-L. Phloem Loading in Vicia Faba Leaves: Effect of N-Ethylmaleimide and Parachloromercuribenzenesulfonic Acid on H+ Extrusion, K+ and Sucrose Uptake. *Planta* **1980**, *149* (2), 144−148.
(33) Li, T.; Takeoka, S. Enhanced Cellular Uptake of Maleimide-Modified Liposomes via Thiol-Mediated Transport. *Int. J. Nanomedicine* **2014**, *9* (1), 2849−2861.
(34) Wenge, B.; Bönisch, H. N-Ethylmaleimide Differentially Inhibits Substrate Uptake by and Ligand Binding to the Noradrenaline Transporter. *Naunyn-Schmied Arch Pharmacol* **2008**, *377* (3), 255−265.
(35) Zhang, H.; Ding, A.; Ye, B.; Wang, Z.; Zhang, J.; Qiu, L.; Chen, J. Carbon Nitride Nanosheets for Imaging Traceable CpG Oligodeoxynucleotide Delivery. *ACS Appl. Nano Mater.* **2021**, *4* (8), 8546−8555.
(36) Di Marzio, L.; Marianecci, C.; Cinque, B.; Nazzarri, M.; Cimini, A. M.; Cristiano, L.; Cifone, M. G.; Alhaique, F.; Carafa, M. PH-Sensitive Non-Phospholipid Vesicle and Macrophage-like Cells: Binding, Uptake and Endocytotic Pathway. *Biochimica et Biophysica Acta (BBA) - Biomembranes* **2008**, *1778* (12), 2749−2756.
(37) Wolfram, J.; Nizzero, S.; Liu, H.; Li, F.; Zhang, G.; Li, Z.; Shen, H.; Blanco, E.; Ferrari, M. A Chloroquine-Induced Macrophage-Preconditioning Strategy for Improved Nanodelivery. *Sci. Rep* **2017**, *7* (1), 13738.
(38) Perry, J. W.; Wobus, C. E. Endocytosis of Murine Norovirus 1 into Murine Macrophages Is Dependent on Dynamin II and Cholesterol. *J. Virol* **2010**, *84* (12), 6163−6176.
(39) Kapetanovic, R.; Nahori, M.-A.; Balloy, V.; Fitting, C.; Philpott, D. J.; Cavaillon, J.-M.; Adib-Conquy, M. Contribution of Phagocytosis and Intracellular Sensing for Cytokine Production by Staphylococcus Aureus-Activated Macrophages. *Infect. Immun.* **2007**, *75* (2), 830−837.
(40) Lim, E. Y.; Park, J.; Kim, Y. T.; Kim, M. J. Imipramine Inhibits Migration and Invasion in Metastatic Castration-Resistant Prostate Cancer PC-3 Cells via AKT-Mediated NF-KB Signaling Pathway. *Molecules* **2020**, *25* (20), 4619.
(41) Sousa de Almeida, M.; Susnik, E.; Drasler, B.; Taladriz-Blanco, P.; Petri-Fink, A.; Rothen-Rutishauser, B. Understanding Nanoparticle Endocytosis to Improve Targeting Strategies in Nanomedicine. *Chem. Soc. Rev.* **2021**, *50* (9), 5397−5434.
(42) Lee, D. J.; Cox, D.; Li, J.; Greenberg, S. Rac1 and Cdc42 Are Required for Phagocytosis, but Not NF-KB-Dependent Gene Expression, in Macrophages Challenged with Pseudomonas Aeruginosa *. *J. Biol. Chem.* **2000**, *275* (1), 141−146.
(43) Massol, P.; Montcourrier, P.; Guillemot, J.-C.; Chavrier, P. Fc Receptor-Mediated Phagocytosis Requires CDC42 and Rac1. *EMBO Journal* **1998**, *17* (21), 6219−6229.
(44) Qu, L.; Wang, Y.; Li, Y.; Wang, X.; Li, N.; Ge, S.; Wang, J.; Wang, G.-J.; Volkow, N. D.; Lang, B.; Wang, P.; Wu, H.; Zeng, J.; Fu, J.; Li, J.; Zhang, Y.; Wang, X. Decreased Neuronal Excitability in Medial Prefrontal Cortex during Morphine Withdrawal Is Associated with Enhanced SK Channel Activity and Upregulation of Small GTPase Rac1. *Theranostics* **2020**, *10* (16), 7369−7383.
(45) Jaynes, J. M.; Sable, R.; Ronzetti, M.; Bautista, W.; Knotts, Z.; Abisoye-Ogunniyan, A.; Li, D.; Calvo, R.; Dashnyam, M.; Singh, A.; Guerin, T.; White, J.; Ravichandran, S.; Kumar, P.; Talsania, K.; Chen, V.; Ghebremedhin, A.; Karanam, B.; Bin Salam, A.; Amin, R.; Odzorig, T.; Aiken, T.; Nguyen, V.; Bian, Y.; Zarif, J. C.; de Groot, A. E.; Mehta, M.; Fan, L.; Hu, X.; Simeonov, A.; Pate, N.; Abu-Asab, M.; Ferrer, M.; Southall, N.; Ock, C.-Y.; Zhao, Y.; Lopez, H.; Kozlov, S.; de Val, N.; Yates, C. C.; Baljinnyam, B.; Marugan, J.; Rudloff, U. Mannose Receptor (CD206) Activation in Tumor-Associated Macrophages Enhances Adaptive and Innate Antitumor Immune Responses. *Science Translational Medicine* **2020**, *12* (530), No. eaax6337.
(46) Zhu, S.; Lu, P.; Liu, H.; Chen, P.; Wu, Y.; Wang, Y.; Sun, H.; Zhang, X.; Xia, Q.; Heng, B. C.; Zhou, Y.; Ouyang, H. W. Inhibition of Rac1 Activity by Controlled Release of NSC23766 from Chitosan Microspheres Effectively Ameliorates Osteoarthritis Development in Vivo. *Ann. Rheum Dis* **2015**, *74* (1), 285−293.
(47) Jay, S. M.; Skokos, E. A.; Zeng, J.; Knox, K.; Kyriakides, T. R. Macrophage Fusion Leading to Foreign Body Giant Cell Formation Persists under Phagocytic Stimulation by Microspheres in in Vitro and in Vivo in Mouse Models. *J. Biomed Mater. Res. A* **2010**, *93* (1), 189−199.
(48) Bennett, M. R.; Gibson, D. F.; Schwartz, S. M.; Tait, J. F. Binding and Phagocytosis of Apoptotic Vascular Smooth Muscle Cells Is Mediated in Part by Exposure of Phosphatidylserine. *Circ. Res.* **1995**, *77* (6), 1136−1142.
(49) van Genderen, H. O.; Kenis, H.; Hofstra, L.; Narula, J.; Reutelingsperger, C. P. M. Extracellular Annexin A5: Functions of Phosphatidylserine-Binding and Two-Dimensional Crystallization. *Biochimica et Biophysica Acta (BBA) - Molecular Cell Research* **2008**, *1783* (6), 953−963.
(50) Yoshida, S.; Minematsu, N.; Chubachi, S.; Nakamura, H.; Miyazaki, M.; Tsuduki, K.; Takahashi, S.; Miyasho, T.; Iwabuchi, T.; Takamiya, R.; Tateno, H.; Mouded, M.; Shapiro, S. D.; Asano, K.; Betsuyaku, T. Annexin V Decreases PS-Mediated Macrophage Efferocytosis and Deteriorates Elastase-Induced Pulmonary Emphysema in Mice. *Am. J. Physiol Lung Cell Mol. Physiol* **2012**, *303* (10), L852−860.
(51) Sheth, V.; Wang, L.; Bhattacharya, R.; Mukherjee, P.; Wilhelm, S. Strategies for Delivering Nanoparticles across Tumor Blood Vessels. *Adv. Funct. Mater.* **2021**, *31* (8), 2007363.
(52) Rennick, J. J.; Johnston, A. P. R.; Parton, R. G. Key Principles and Methods for Studying the Endocytosis of Biological and Nanoparticle Therapeutics. *Nat. Nanotechnol.* **2021**, *16* (3), 266−276.
(53) Hossen, Md. N.; Wang, L.; Chinthalapally, H. R.; Robertson, J. D.; Fung, K.-M.; Wilhelm, S.; Bieniasz, M.; Bhattacharya, R.; Mukherjee, P. Switching the Intracellular Pathway and Enhancing the Therapeutic Efficacy of Small Interfering RNA by Auroliposome. *Science Advances* **2020**, *6* (30), No. eaba5379.
(54) Tian, T.; Zhu, Y.-L.; Zhou, Y.-Y.; Liang, G.-F.; Wang, Y.-Y.; Hu, F.-H.; Xiao, Z.-D. Exosome Uptake through Clathrin-Mediated Endocytosis and Macropinocytosis and Mediating MiR-21 Delivery. *J. Biol. Chem.* **2014**, *289* (32), 22258−22267.
(55) Biddeci, G.; Spinelli, G.; Massaro, M.; Riela, S.; Bonaccorsi, P.; Barattucci, A.; Di Blasi, F. Study of Uptake Mechanisms of Halloysite Nanotubes in Different Cell Lines. *Int. J. Nanomedicine* **2021**, *16*, 4755−4768.
(56) Rippe, M.; Stefanello, T. F.; Kaplum, V.; Britta, E. A.; Garcia, F. P.; Poirot, R.; Companhoni, M. V. P.; Nakamura, C. V.; Szarpak-Jankowska, A.; Auzély-Velty, R. Heparosan as a Potential Alternative to


https://doi.org/10.1021/acs.nanolett.2c02226
Nano Lett. XXXX, XXX, XXX−XXX

Hyaluronic Acid for the Design of Biopolymer-Based Nanovectors for Anticancer Therapy. *Biomater. Sci.* **2019**, *7* (7), 2850−2860.
(57) Jackson, D. G. Hyaluronan in the Lymphatics: The Key Role of the Hyaluronan Receptor LYVE-1 in Leucocyte Trafficking. *Matrix Biol.* **2019**, *78*−*79*, 219−235.
(58) *Essentials of Glycobiology*, 3rd ed.; Varki, A., Cummings, R. D., Esko, J. D., Stanley, P., Hart, G. W., Aebi, M., Darvill, A. G., Kinoshita, T., Packer, N. H., Prestegard, J. H., Schnaar, R. L., Seeberger, P. H., Eds.; Cold Spring Harbor Laboratory Press: Cold Spring Harbor (NY), 2015.
(59) Chavaroche, A. A. E.; van den Broek, L. A. M.; Eggink, G. Production Methods for Heparosan, a Precursor of Heparin and Heparan Sulfate. *Carbohydr. Polym.* **2013**, *93* (1), 38−47.
(60) Nikitovic, D.; Assouti, M.; Sifaki, M.; Katonis, P.; Krasagakis, K.; Karamanos, N. K.; Tzanakakis, G. N. Chondroitin Sulfate and Heparan Sulfate-Containing Proteoglycans Are Both Partners and Targets of Basic Fibroblast Growth Factor-Mediated Proliferation in Human Metastatic Melanoma Cell Lines. *International Journal of Biochemistry & Cell Biology* **2008**, *40* (1), 72−83.
(61) de Vet, E. C. J. M.; Newland, S. A. B.; Lyons, P. A.; Aguado, B.; Campbell, R. D. The Cell Surface Receptor G6b, a Member of the Immunoglobulin Superfamily, Binds Heparin. *FEBS Lett.* **2005**, *579* (11), 2355−2358.
(62) DeAngelis, P. L. Heparosan, a Promising 'Naturally Good' Polymeric Conjugating Vehicle for Delivery of Injectable Therapeutics. *Expert Opinion on Drug Delivery* **2015**, *12* (3), 349−352.
(63) Soares da Costa, D.; Reis, R. L.; Pashkuleva, I. Sulfation of Glycosaminoglycans and Its Implications in Human Health and Disorders. *Annu. Rev. Biomed. Eng.* **2017**, *19* (1), 1−26.
(64) *Natural and Synthetic Biomedical Polymers*, 1st ed.; Kumbar, S., Laurencin, C., Deng, M., Eds.; Elsevier: Amsterdam; Boston, 2014; pp 71−73.
(65) Fujimoto, T.; Kawashima, H.; Tanaka, T.; Hirose, M.; Toyama-Sorimachi, N.; Matsuzawa, Y.; Miyasaka, M. CD44 Binds a Chondroitin Sulfate Proteoglycan, Aggrecan. *Int. Immunol.* **2001**, *13* (3), 359−366.
(66) Hirose, J.; Kawashima, H.; Swope Willis, M.; Springer, T. A.; Hasegawa, H.; Yoshie, O.; Miyasaka, M. Chondroitin Sulfate B Exerts Its Inhibitory Effect on Secondary Lymphoid Tissue Chemokine (SLC) by Binding to the C-Terminus of SLC. *Biochim. Biophys. Acta* **2002**, *1571* (3), 219−224.
(67) Zhang, Q.; Du, Y.; Chen, J.; Xu, G.; Yu, T.; Hua, X.; Zhang, J. Investigation of Chondroitin Sulfate D and Chondroitin Sulfate E as Novel Chiral Selectors in Capillary Electrophoresis. *Anal Bioanal Chem.* **2014**, *406* (5), 1557−1566.
(68) Mikami, T.; Yasunaga, D.; Kitagawa, H. Contactin-1 Is a Functional Receptor for Neuroregulatory Chondroitin Sulfate-E*. *J. Biol. Chem.* **2009**, *284* (7), 4494−4499.
(69) Singh, B.; Maharjan, S.; Kim, Y.-K.; Jiang, T.; Islam, M. A.; Kang, S.-K.; Cho, M.-H.; Choi, Y.-J.; Cho, C.-S. Targeted Gene Delivery via N-Acetylglucosamine Receptor Mediated Endocytosis. *J. Nanosci Nanotechnol* **2014**, *14* (11), 8356−8364.
(70) Sindhwani, S.; Syed, A. M.; Ngai, J.; Kingston, B. R.; Maiorino, L.; Rothschild, J.; MacMillan, P.; Zhang, Y.; Rajesh, N. U.; Hoang, T.; Wu, J. L. Y.; Wilhelm, S.; Zilman, A.; Gadde, S.; Sulaiman, A.; Ouyang, B.; Lin, Z.; Wang, L.; Egeblad, M.; Chan, W. C. W. The Entry of Nanoparticles into Solid Tumours. *Nat. Mater.* **2020**, *19* (5), 566−575.
(71) Dai, Q.; Wilhelm, S.; Ding, D.; Syed, A. M.; Sindhwani, S.; Zhang, Y.; Chen, Y. Y.; MacMillan, P.; Chan, W. C. W. Quantifying the Ligand-Coated Nanoparticle Delivery to Cancer Cells in Solid Tumors. *ACS Nano* **2018**, *12* (8), 8423−8435.
(72) Wilhelm, S.; Hirsch, T.; Patterson, W. M.; Scheucher, E.; Mayr, T.; Wolfbeis, O. S. Multicolor Upconversion Nanoparticles for Protein Conjugation. *Theranostics* **2013**, *3* (4), 239−248.
(73) Donahue, N. D.; Francek, E. R.; Kiyotake, E.; Thomas, E. E.; Yang, W.; Wang, L.; Detamore, M. S.; Wilhelm, S. Assessing Nanoparticle Colloidal Stability with Single-Particle Inductively Coupled Plasma Mass Spectrometry (SP-ICP-MS). *Anal Bioanal Chem.* **2020**, *412* (22), 5205−5216.
(74) Narum, S. M.; Le, T.; Le, D. P.; Lee, J. C.; Donahue, N. D.; Yang, W.; Wilhelm, S.Chapter 4 - Passive Targeting in Nanomedicine: Fundamental Concepts, Body Interactions, and Clinical Potential. In *Nanoparticles for Biomedical Applications: Fundamental Concepts, Biological Interactions and Clinical Applications*; Chung, E. J., Leon, L., Rinaldi, C., Eds.; Elsevier, 2020; pp 37−53 DOI: 10.1016/B978-0-12-816662-8.00004-7.
(75) Lee, J. C.; Donahue, N. D.; Mao, A. S.; Karim, A.; Komarneni, M.; Thomas, E. E.; Francek, E. R.; Yang, W.; Wilhelm, S. Exploring Maleimide-Based Nanoparticle Surface Engineering to Control Cellular Interactions. *ACS Appl. Nano Mater.* **2020**, *3* (3), 2421−2429.
(76) Suk, J. S.; Xu, Q.; Kim, N.; Hanes, J.; Ensign, L. M. PEGylation as a Strategy for Improving Nanoparticle-Based Drug and Gene Delivery. *Adv. Drug Deliv Rev.* **2016**, *99* (Pt A), 28−51.


https://doi.org/10.1021/acs.nanolett.2c02226
*Nano Lett.* XXXX, XXX, XXX−XXX